CHAPTER VI

THE EFFECTS OF THERMODYNAMIC PARAMETERS ON MASS TRANSFER AND ENANTIOSEPARATION OF (*R,S*)-AMLODIPINE ACROSS A HOLLOW FIBER SUPPORTED LIQUID MEMBRANE

Niti Sunsandee [a], Natchanun Leepipatpiboon [b,*], Prakorn Ramakul [c], Thidarat Wongsawa [a], Ura Pancharoen [a,**]

[a] *Department of Chemical Engineering, Faculty of Engineering, Chulalongkorn University, Bangkok 10330, Thailand.*

[b] *Chromatography and Separation Research Unit, Department of Chemistry, Faculty of Science, Chulalongkorn University, Patumwan, Bangkok 10330, Thailand.*

[c] *Department of Chemical Engineering, Faculty of Engineering and Industrial Technology, Silpakorn University, Nakhon Pathom 73000, Thailand.*

This article has been published in Journal: Separation and Purification Technology. Page: 50-61. Volume: 120. Year: 2013.

6.1 ABSTRACT

Chiral separation of enantiomers of amlodipine, one of the most commonly prescribed antihypertensive drugs, was examined using the hollow fiber supported liquid membrane (HFSLM) extraction technique. The influence of temperature on enantioseparation of (*R,S*)-amlodipine via a HFSLM containing the chiral selector *O,O'*-dibenzoyl-(2*S*,3*S*)-tartaric acid ((+)-DBTA) was systematically investigated. The parameters affecting the mass transfer such as distribution ratio and flux were determined at different temperatures ranging from 278.15 K to 313.15 K. The thermodynamic parameters, ΔH and ΔG, were determined, and an interesting relationship with stoichiometric value was found: higher temperatures lead to an increase in distribution ratio but a decrease in enantioselectivity. The activation energy (E_a) of the (*S*)-amlodipine extraction reaction was 71.10 kJ/mol. The chemical reaction between (*S*)-amlodipine and (+)-DBTA is the mass transfer-controlling step for the enantioseparation of (*S*)-amlodipine by a hollow fiber supported liquid membrane system.

6.2 INTRODUCTION

Amlodipine–3-ethyl-5-methyl-2-[(-2-(aminoethoxymethyl]-4-(2-chloro-phenyl)-1,4-dihydro-6-methyl-3,5-pyridinedicarboxylate (Figure 6.1) – is a potent third-generation dihydropyridine derivative calcium channel blocker used in the treatment of hypertension and angina pectoris [1]. Like most other calcium blocker agents of the dihydropyridine type, amlodipine is therapeutically used as a racemic mixture. However, the vasodilating effect only resides in (*S*)-amlodipine [2]. (*R*)-amlodipine is inactive, and is thought to be responsible for pedal edema observed with racemic amlodipine [3]. (*S*)-amlodipine is the more potent calcium channel blocker showing about 2,000 times the potency in *in vitro* evaluation in the rat aorta than (*R*)-amlodipine [4]. In addition to its longer duration of action, (*S*)-amlodipine reduces the chances of reflex tachycardia, and its clearance is subject to much less inter-subject variation than (*R*)-amlodipine [5].

Several methods dedicated to the separation of enantiomers of amlodipine have been reported [6]. Separation techniques such as crystallization [7], chromatography [8] and capillary electrophoresis [9] have been developed. These techniques have furthered research and development into the separation of (*S*)-amlodipine from its racemic mixture; however, there are some deficiencies. Crystallization requires many time-consuming and cost-inefficient steps [10]. Chromatography and capillary electrophoresis are not suitable for production of multi-gram-quantities [11]. Membrane extraction is one of the separation processes, which combines liquid-liquid extraction [12-16] with a membrane [17]. The literature on enantioselective liquid-liquid extraction spans more than half a century of research [18-21]. Enantioseparation through liquid membranes was first reported in the 1970s [22]. Recently, enantioselection by membrane-supported liquid-liquid extraction has been a technology of interest for chemical engineers in a wide range of fields, such as fine chemicals, pharmaceuticals and foods [23-25]. Hollow fiber supported liquid membrane (HFSLM) extraction is an especially popular technique. Great progress has been made in such applications, as in metal ion extraction [26, 27], organic extraction [28], pharmaceutical extraction [29], and enzymatic transformation [30]. In recent years, racemic separation by HFSLM has proven to be a topic of great interest [31, 32].

HFSLM is renowned as an effective method for simultaneous extraction and recovery of compounds from very dilute solutions of a component of interest in the feed by a single unit operation [33]. The advantages of the hollow fiber contactor over traditional separation techniques include lower capital and operating costs [34], lower energy consumption [35], less solvent used [36] and high selectivity [37]. An HFSLM is thus considered suitable for treatment of chemical synthesis-based pharmaceutical wastewater.

The objective of this study was to investigate the effects of temperature on mass transfer in a single hollow fiber supported liquid membrane extraction. The use of a hollow fiber module in liquid membrane extraction is now seen as a popular choice [38, 39] because of its simplicity, low cost, and ability to provide high enrichment factors. However, very few studies have been conducted on the influence of temperature in such a module [40, 41]. Most of these have investigated the effects

of temperature in bulk liquid membranes [42, 43] or flat-sheet modules [44]. Temperature has a major impact on enantioselective separation [23, 45-47]. Van't Hoff analysis of enantioselectivity values derived from variable temperatures studies are routinely used to assess thermodynamic functions of enantioselective separation. This may be interpreted in terms of mechanistic aspects of chiral recognition.

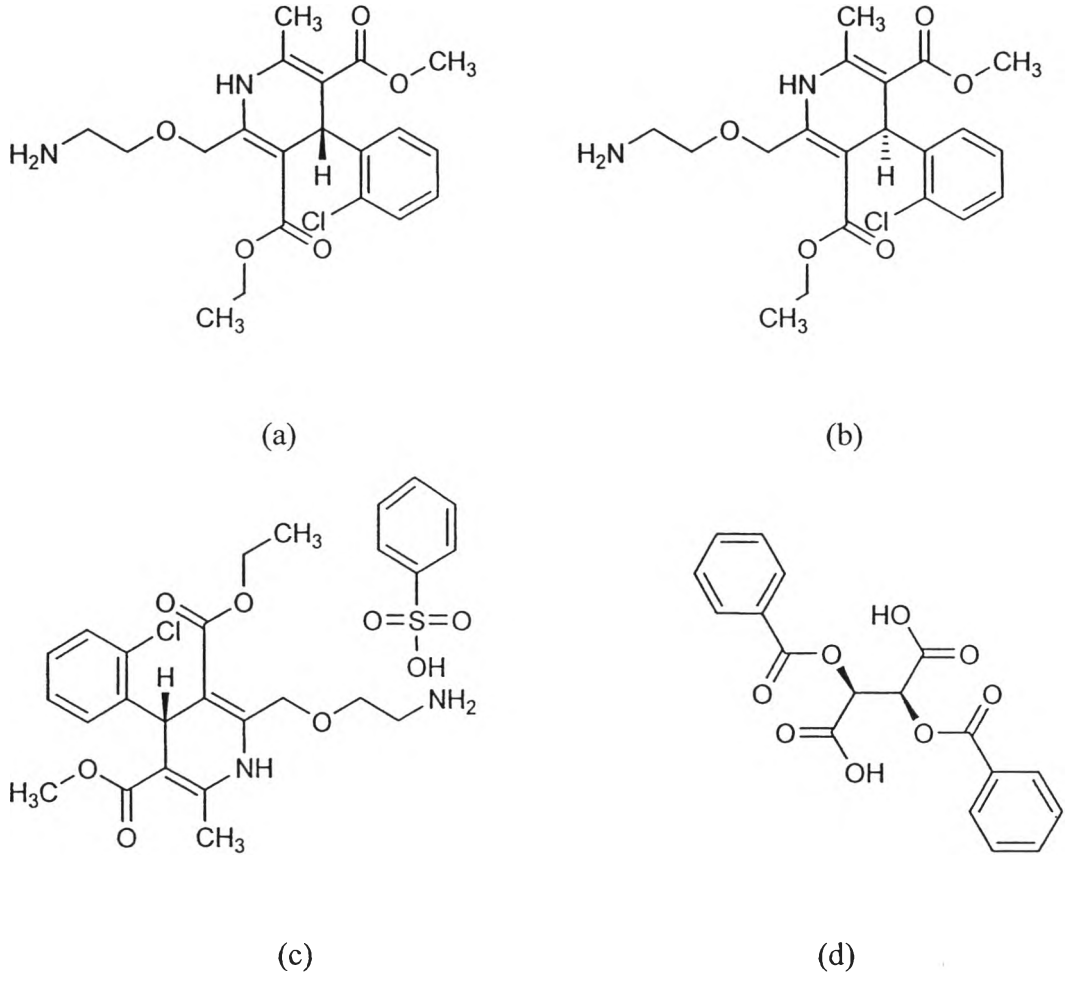

Figure 6.1 Structures of (a) (*S*)-amlodipine, (b) (*R*)-amlodipine
(c) (*S*)-amlodipine benzenesulfonate, (d) *O,O'*--dibenzoyl-(2*S*, 3*S*)-tartaric acid

6.3 THEORY

The supported chiral liquid membrane consists of an organic solution of a chiral selector as the extractant, which is held in polymeric micropores by capillary action [48]. The enantioselector *O,O'*-dibenzoyl-(2*S*,3*S*)-tartaric acid ((+)-DBTA) resides in the liquid membrane, trapped in the hydrophobic microporous hollow-fiber module. (+)-DBTA forms enantioselective complexes with (*S*)-amlodipine by hydrogen bonding [49]. The transport mechanism of (*S*)-amlodipine through the liquid membrane is shown in Figure 6.2.

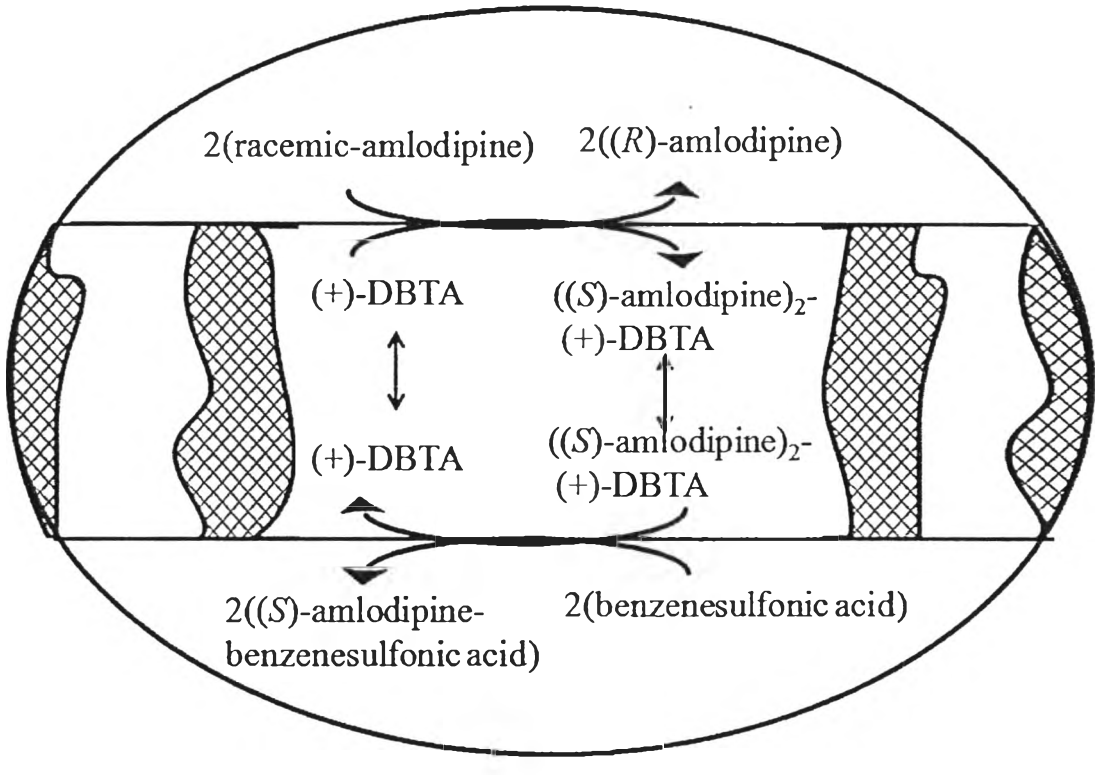

Figure 6.2 Transport scheme for chiral extractant

The mechanism and the enantioselective transport kinetics scheme of amlodipine enantiomers through a hollow fiber supported liquid membrane are described in Eqs. (6.1) and (6.2):

$$2[(S)\text{-amlodipine}]_f + [(+)\text{-DBTA}]_m \underset{k_2}{\overset{k_1}{\rightleftharpoons}} [[(S)\text{-amlodipine}]_2\text{-}(+)\text{-DBTA}]_m \quad (6.1)$$

where k_1 and k_2 are the apparent rate constants of feed-membrane interfacial transport and membrane-strip interfacial transport of amlodipine enantiomers, respectively. The indices suffixes, f and m, indicate feed phase and membrane phase, respectively.

Benzenesulfonic acid reacts with $[[(S)\text{-amlodipine}]_2\text{-}(+)\text{-DBTA}]_m$ to recover (*S*)-amlodipine into the stripping phase:

$$[[(S)\text{-amlodipine}]_2\text{-}(+)\text{-DBTA}]_m + 2[\text{benzenesulfonic acid}]_s \quad (6.2)$$

$$\underset{k_4}{\overset{k_3}{\rightleftharpoons}} \; 2[(S)\text{-amlodipine-benzenesulfonate}]_s + [(+)\text{-DBTA}]_m$$

where k_3 and k_4 are the apparent rate constants of feed-membrane interfacial transport and membrane-strip interfacial transport of amlodipine enantiomers, respectively. The indices suffixes, m and s, indicate membrane phase and stripping solution phase, respectively.

6.3.1 Extraction equilibrium constant and distribution ratio

The extraction equilibrium constant ($K_{ex(S)}$) of (*S*)-amlodipine extracted by (+)-DBTA can be written as:

$$K_{ex} = \frac{[[(S)\text{-amlodipine}]_2\text{-}(+)\text{-DBTA}]_m}{[(S)\text{-amlodipine}]_f^2[(+)\text{-DBTA}]_m} \quad (6.3)$$

The enantioselectivity of a process may be expressed as the operational selectivity [45]. For the current system, (*S*)-amlodipine is preferentially extracted. The distribution ratios of (*S*)-amlodipine and (*R*)-amlodipine, D_S and D_R, respectively, extracted from the feed phase into the membrane phase were determined as in Eqs. (6.1) and (6.2).

The distribution ratio for (*S*)-amlodipine (D_S) is given by:

$$D = \frac{[[(S)\text{-amlodipine}]_2\text{-}(+)\text{-DBTA}]_m}{[(S)\text{-amlodipine}]_f} \tag{6.4}$$

The distribution ratio for (*R*)-amlodipine D_R is given by:

$$D_R = \frac{[[(R)\text{-amlodipine}]_2\text{-}(+)\text{-DBTA}]_m}{[(R)\text{-amlodipine}]_f} \tag{6.5}$$

According to Eq. (6.4), the distribution ratio could then be derived as a function of the extraction equilibrium constant as follows:

$$D_S = K_{ex(S)}[(S)\text{-amlodipine}]_f[(+)\text{-DBTA}]_m \tag{6.6}$$

The selectivity is defined as enantioselectivity. The enantioselectivity of the membrane process is given in terms of the separation factor (α) and the enantiomeric excess (% *e.e.*). Enantioselectivity is one of the important parameters for estimating the extraction performance of the extractant, which can be calculated by the following formulae:

$$\alpha = \frac{D_S}{D_R} \tag{6.7}$$

In this work, the extractability of (*S*)-amlodipine was determined by the percentage of extraction:

$$\%e.e. = \frac{|D_S - D_R|}{(D_S + D_R)} \times 100 \tag{6.8}$$

$$\%\text{Extraction} = \frac{C_{f,in} - C_{f,out}}{C_{f,in}} \times 100 \tag{6.9}$$

The percentage of recovery was calculated by:

$$\%\text{Stripping} = \frac{C_{s,out}}{C_{f,in}} \times 100 \tag{6.10}$$

where $C_{f,in}$ and $C_{f,out}$ are the inlet and outlet feed concentrations of component i (mmol/L), and $C_{s,in}$ is the outlet stripping concentration of component i (mmol/L).

6.3.2 The effect of temperature on extraction equilibrium

The effect of temperature on the extraction equilibrium ($K_{ex(S)}$) of (*S*)-amlodipine extracted with (+)-DBTA is directly related to the Van't Hoff equation. This equation has a connection with the standard Gibbs free-energy and Gibbs–Helmholtz equations [50, 51].

Gibbs free-energy change (ΔG^0) for the extraction can be calculated from:

$$\Delta G^{0}_{ex(S)} = -RT \ln K_{ex(S)} \tag{6.11}$$

$$\Delta G^{0}_{D_S} = -RT \ln D_S \tag{6.12}$$

$$\Delta G^{0}_{D_R} = -RT \ln D_R \tag{6.13}$$

$$\Delta G^{0}_{\alpha} = -RT \ln \alpha \tag{6.14}$$

$$\ln K_{ex(S)} = -\frac{\Delta G^{0}_{ex(S)}}{RT} \tag{6.15}$$

However, since activity coefficients have not been incorporated, shifted free energy, $\Delta G^{0}_{ex(S)}$, can be calculated. Gibb's free-energy change ($\Delta G^{0}_{ex(S)}$) is related to the standard enthalpy and extraction entropy changes ($\Delta H^{0}_{ex(S)}$ and $\Delta S^{0}_{ex(S)}$) through the

Gibbs–Helmholtz equation. The relationship between Gibbs free energy and the enthalpy and entropy is as follows in Eq. (6.16).

$$\Delta G^0 = \Delta H^0 - T\Delta S^0 \tag{6.16}$$

Substituting Eq. (6.16) into Eq. (6.15) results in the Van't Hoff equation in linear form, and is shown as Eq. (6.17):

$$\ln K_{ex(S)} = -\frac{\Delta H^0_{ex(S)}}{RT} + \frac{\Delta S^0_{ex(S)}}{R} \tag{6.17}$$

A plot of ln $K_{ex(S)}$ versus $1/T$ should give a straight line, with the standard enthalpy change calculated from the slope. The equilibrium constant is proportional to $K_{ex(S)}$. Thus, slopes of ln $K_{ex(S)}$ vs $1/T$ plots would yield standard enthalpy change [52, 53]. Previous works discussed the conditions for the constancy of $\Delta H^0_{ex(S)}$ and $\Delta S^0_{ex(S)}$, and these apply here as well [54–56].

6.3.3 Permeability coefficient

The permeation of (*S*)-amlodipine can be expressed in terms of the permeability coefficient (*P*), as proposed by Danesi [57] in Eq. (18):

$$-V_f \ln\left(\frac{C_f}{C_{f,o}}\right) = AP\frac{\beta}{\beta+1}t \tag{6.18}$$

where P is the permeability coefficient (cm/s), V_f is the volume of the feed (cm^3), $C_{f,0}$ is the (*S*)-amlodipine concentration (mol/L) in initial time (t = 0), C_f is the (*S*)-amlodipine concentration at time t (mol/L), A is the effective area of the hollow fiber module (cm^2), t is the time (min).

$$\beta = \frac{Q_f}{PL\varepsilon\pi N r_i} \tag{6.19}$$

$AP(\beta/(\beta + 1))$ is the slope of the plot between $-V_f \ln (C_f/C_{f,0})$ versus t in Eq. (6.18), and P can be obtained by Eq. (6.19), where Q_f is the volumetric flow rate of feed solution (cm^3/s), L is the length of the hollow fiber (cm), ε is the porosity of the hollow fiber (%), N is number of hollow fibers in the module and r_i is the internal radius of the hollow-fiber module (cm).

To determine mass-transfer coefficients for (*S*)-amlodipine enantio-separation by HFSLM, the mass-transfer model and permeability coefficient (P) are employed. The permeability coefficient depends on mass transfer resistance, which is the reciprocal of the mass-transfer coefficients as follow

$$\frac{1}{P} = \frac{1}{k_f} + \frac{r_i}{r_{lm}}\frac{1}{P_m} + \frac{r_i}{r_o}\frac{1}{k_s} \tag{6.20}$$

where r_{lm} is the log-mean radius of the hollow fiber, r_o is the external radius of the hollow fiber module (cm), k_f is the aqueous mass-transfer coefficient in the tube side, k_s is the stripping mass-transfer coefficient in the shell side, and P_m is the membrane permeability coefficient.

The relationship between P_m and the distribution ratio (D_S) is as follows:

$$P_m = Dk_m \tag{6.21}$$

Combining Eq. (6.6) and Eq. (6.21), thus:

$$P_m = K_{ex}\, k_m [(S)\text{-amlodipine}]_f [(+)\text{-DBTA}]_n \tag{6.22}$$

where k_m is the mass-transfer coefficient of the membrane, and the value of the liquid-membrane permeability coefficient (P_m) from Eq. (6.22) is substituted into Eq. (6.20).

Assuming that the stripping reaction is instantaneous and the contribution of the stripping phase is neglected, Eq. (6.20) becomes:

$$\frac{1}{P} = \frac{1}{k_f} + \frac{r_i}{r_{lm}} \frac{1}{K_{ex}\, k_m [(S)\text{-amlodipine}]_f [(+)\text{-DBTA}]_m} \tag{6.23}$$

where k_f is the mass transfer coefficient of the feed solution.

6.3.4 Activation energy values (E_a)

The activation energy values were obtained from the Arrhenius equation, as shown in Eq. (6.24). Activation energy (E_a) values have a strong effect on the temperature of actual rate constants. E_a values are usually below 20 kJ/mol. These values are generally accepted as indicative of pure diffusion-limited transport. When the activation energies are higher than 40 kJ/mol, the chemical reactions play a role in the transport [58, 59]. The activation energy of the transport of (*S*)-amlodipine in the HFSLM system was obtained by plotting the flux (*J*) values vs. (1/*T*) [60–62], using Eq. (6.25):

$$J = Ae^{-E_a/RT} \tag{6.24}$$

$$\ln J = \ln A - \frac{E_a}{R}\frac{1}{T} \tag{6.25}$$

where J is the flux, R denotes the universal gas constant (8.3145 J/mol·K), A is the frequency factor, E_a is the activation energy and T is the absolute temperature.

According to the definition of flux given by Lin and Juang [63], the flux of (*S*)-amlodipine can be presented as Eq. (6.26):

$$J = -\frac{d[(S)-\text{amlodipine}]_f}{dt}\frac{V}{A} \tag{6.26}$$

where V is the volume of the feed solution (cm^3) and A is the membrane area (cm^2).

6.4 EXPERIMENT

6.4.1 Chemicals and reagents

Pharmaceutical-grade (*R*)-amlodipine, (*S*)-amlodipine and racemic amlodipine were provided by the Government Pharmaceutical Organization (GPO) of Thailand. *O,O'*-dibenzoyl-(2*S*,3*S*)-tartaric acid ((+)-DBTA) was obtained from Acros Organics (Geel, Belgium). The solvents *N,N*-dimethylformamide, cyclohexane, 1-decanol and 1-propanol, all of analytical reagent grade, were purchased from Merck, Germany. All reagents used in this experiment were GR grade (Merck). Aqueous solutions were prepared using Milli-Q® deionized water (Millipore, Billerica MA, USA). Doubly deionized water was used throughout the experiments.

6.4.2 Apparatus

The hollow fiber supported liquid membrane (HFSLM) system (Liqui-Cel® Extra-Flow 2.5 × 8 inch membrane contactor) was manufactured by Celgard (formerly Hoechst Celanese), Charlotte NC, USA. The module uses Celgard® microporous polypropylene fibers that are woven into fabric and wrapped around a central tube feeder that supplies the shell-side fluid. The woven fabrics provide more uniform fiber spacing, which in turn leads to higher mass-transfer coefficients than those obtained with individual fibers [64]. The properties of the hollow-fiber module are specified in Table 6.1. The fibers were put into a solvent-resistant polyethylene tube sheet with polypropylene shell casing.

Table 6.1 Physical characteristics of the hollow fiber module

Properties	Descriptions
Material	Polypropylene
Inside diameter of hollow fiber	240 μm
Outside diameter of hollow fiber	300 μm
Effective length of hollow fiber	15 cm
Number of hollow fibers	35,000
Average pore size	0.03 μm
Porosity	30%
Effective surface area	1.4×10^4 cm^2
Area per unit volume	29.3 cm^2/cm^3
Module diameter	6.3 cm
Module length	20.3 cm
Contact area	30%
Tortuosity factor	2.6
Operating temperature	273.15-333.15 K

6.4.3 Procedures

The single-module operation is shown in Figure 6.3. The selected organic carrier (+)-DBTA was dissolved in 1-decanol (500 mL) and then pumped simultaneously into the tube and shell sides of the hollow-fiber module for 40 min to ensure that the extractant was entirely embedded in the micro pores of the hollow fibers. Subsequently, 5 L (each) of feed solution and stripping solution were fed counter-currently into the tube and shell sides of the module.

The concentration of feed solution was deliberately varied to find the optimum value for (*S*)-amlodipine extraction. The concentration of chiral selector ((+)-DBTA)) in the liquid membrane, volumetric flow rates of feed and stripping solutions, the number of separation cycles, and stability of HFSLM were each investigated in turn. The operating time for each operation was 50 min for one cycle.

The experiments were run at temperatures of 278.15, 283.15, 288.15, 293.15, 298.15, 303.15, 308.15 and 313.15 K. The experimental samples were investigated in two measuring regimes. First, the experimental data in the regime before reaching equilibrium determined the mass transfer parameters. Secondly, the measured data in the regime after equilibrium state determined the thermodynamic parameters. The concentrations of (*S*)-amlodipine and (*R*)-amlodipine in samples from the feed and stripping solutions were determined by high-performance liquid chromatography (HPLC), in accordance with U.S. Patent No. 6646131 B2 [65], to estimate the percentages of extraction and stripping. To achieve higher enantioseparation and to study membrane stability, the number of separation cycles was varied. The feed of the second cycle was obtained from the first outlet feed solution and so on, whereas the inlet stripping solution was fresh.

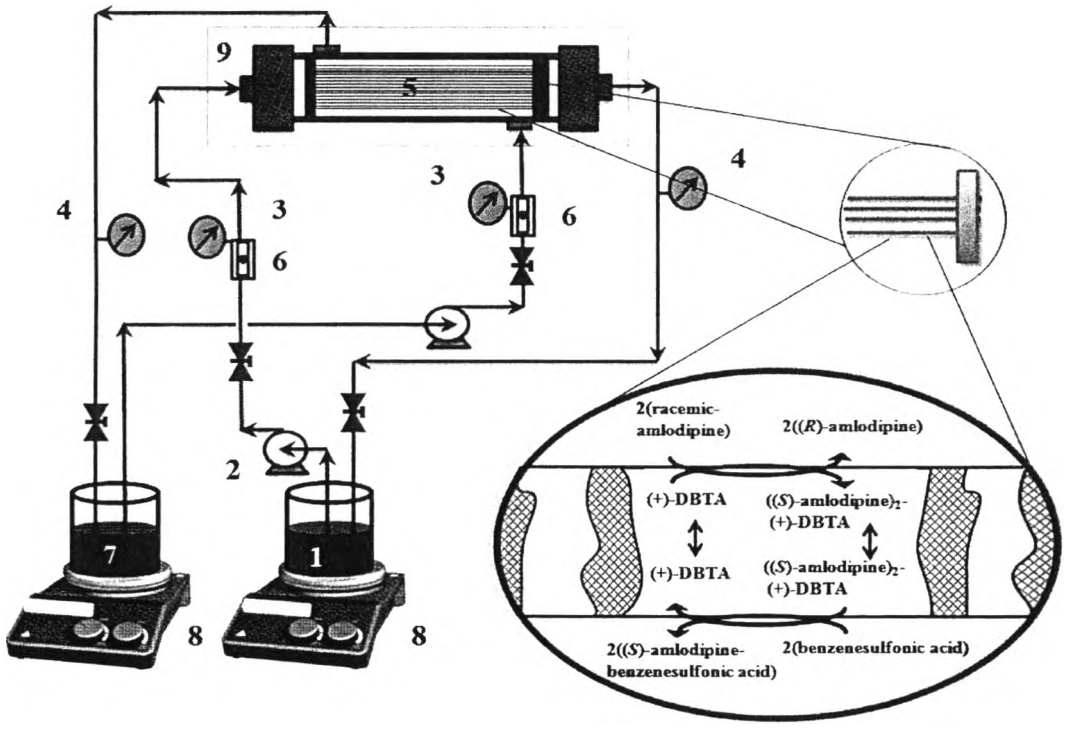

Figure 6.3 Schematic representation of the counter-current flow diagram for batch-mode operation in HFSLM: 1) feed reservoir, 2) gear pumps, 3) inlet pressure gauges, 4) outlet pressure gauges, 5) the hollow-fiber module, 6) flow meters, 7) stripping reservoir, 8) stirrer with temperature controller, and 9) temperature control box

6.4.4 Analytical instruments and chromatographic conditions

The chromatographic system consisted of an Agilent 1100 series compact LC system (Agilent Technologies, Palo Alto, CA, USA), equipped with a built-in solvent degasser, quaternary pump, column compartment, photodiode array detector with variable injector, and autosampler. Data analysis was carried out using ChemStation Version B.04.01 software (Agilent).

The chromatographic procedure was carried out using an Agilent Ultron ES-OVM ovomucoid chiral column (5 μm, 4.6 ×150 mm) [65]. The column was thermostated at 298.15 K by using a column heater. The mobile phase was a mixture of disodium hydrogen phosphate buffer (20 mmol/L) and acetonitrile (80:20 %v/v). The flow rate of the mobile phase was 0.3 mL/min. The injection volume was 20 μL. The detector spectrophotometer was set at UV 237 nm. The relative retention times of (*R*)-amlodipine and (*S*)-amlodipine were about 1.0 and 1.2, respectively. The analysis time was set at 20 min per sample to eliminate potential interference from late eluting peaks. The pH of the aqueous phase was measured with a SevenMulti™ modular pH meter with expansion unit (Mettler-Toledo, Greifensee, Switzerland).

6.5 RESULTS AND DISCUSSION

6.5.1 Optimization of HFSLM extraction for thermodynamic parameters and mass-transfer parameters studies

The extraction efficiency gives the overall mass transfer of the analytes diffusing across HFSLM extraction technique. This is controlled by several parameters, such as: the pH, the concentration and the flow rate of the feed phase; the chiral selector concentration, the phase concentration and the flow rate of the stripping solution, and the number of separation cycles through the hollow-fiber module. The optimal operation is shown in Table 6.2 [49]. Some of these parameters can be determined by examining the physical properties of the compounds. The optimized pH of feed phase was operated at pH 5.0. The concentration of feed phase was 4 mmol/L. The membrane phase ((+)-DBTA) and stripping phase

(benzenesulfonic acid) concentrations were also 4 mmol/L. The feed and stripping solution flow rates were 100 mL/min [49]. The experiments were run for 50 min by recycling the feed flow into the feed storage container and the stripping solution flow into the stripping storage container. In our previous work [49], we found that after 50 min the equilibrium was achieved between the feed phase, the membrane, and the strip phase. The concentration profiles of (*S*)-amlodipine and (*R*)-amlodipine in the retentate and strip phases as a function of time are shown Figure 6.4. In this work, the experiments were investigated in two measuring regimes. First, the experimental data in the regime before reaching equilibrium determined the mass transfer parameters, as explained in sections 6.5.7–6.5.8. Secondly, the measured data in the regime after equilibrium state determined the thermodynamic parameters described in sections 6.5.2–6.5.6.

Table 6.2 Optimized operation using HFSLM in enantioseparation

Phase	Chemical reagent	Concentration	Flow rate
Feed	(*R*,*S*)-amlodipine pKa = 8.6 at 298.15 K	4 mmol/L	100 mL/min
Membrane	*O*,*O*'-dibenzoyl-(2*S*,3*S*) -tartaric acid	4 mmol/L	-
Stripping	benzenesulfonic acid	4 mmol/L	100 mL/min

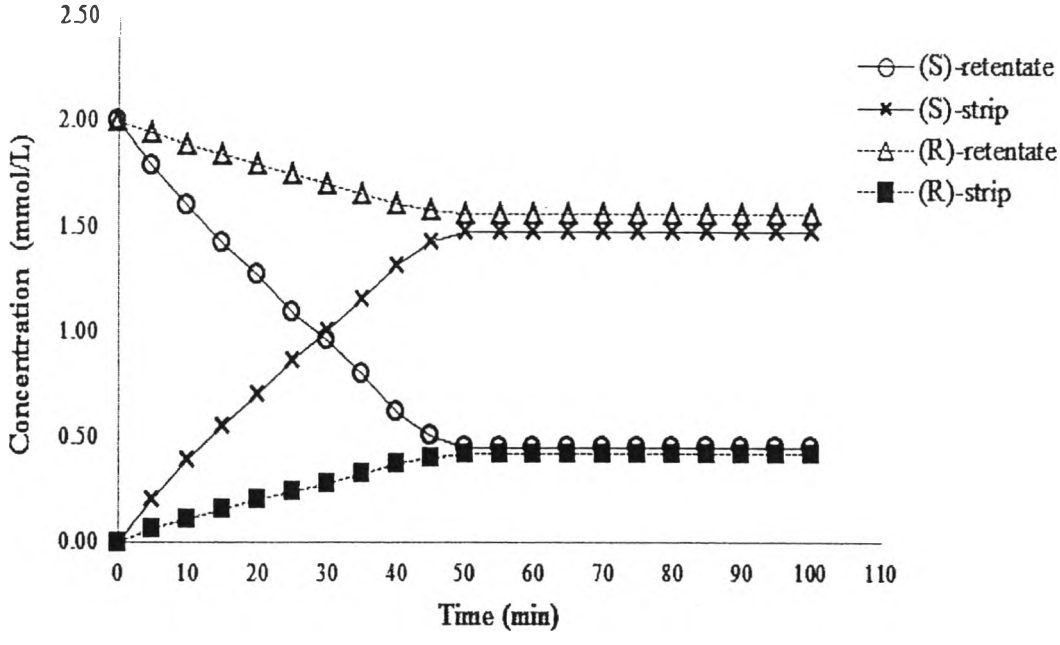

Figure 6.4 The concentration profile of (*S*)-amlodipine and (*R*)-amlodipine in the retentate and strip phases in function of time

6.5.2 Influence of temperature on percentages of extraction, stripping and enantiomeric excess

The feed and stripping solutions were studied at temperatures of 278.15, 283.15, 288.15, 293.15, 298.15, 303.15, 308.15 and 313.15 K to investigate the effects of temperature on the percentages of extraction, stripping, and enantiomeric excess, as shown in Figure 4.5. The optimal conditions were pH 5.0, 4 mmol/L feed solution, 4 mmol/L (+)-DBTA, and 4 mmol/L benzenesulfonic acid. The feed solution flow rate was 100 mL/min and the stripping solution flow rate was 100 mL/min. In Figure 6.5, it can be observed that the enantiomeric excess of (*S*)-amlodipine increased as the temperature decreased. The resulting data at a temperature of 273.15 K show the highest percentage of enantiomeric excess of (*S*)-amlodipine (about 59.50%). The highest percentages of (*S*)-amlodipine extraction and stripping were 81.50% and 74.80%, respectively.

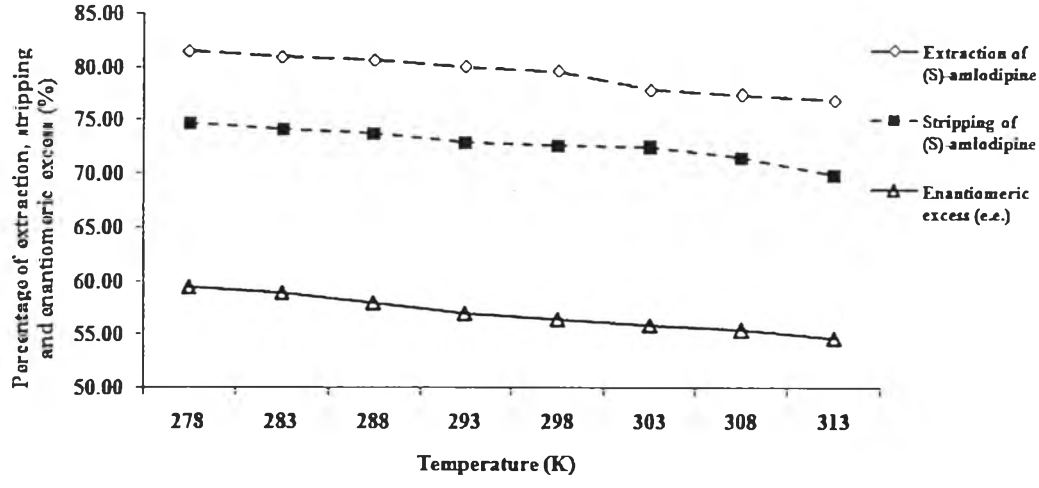

Figure 6.5 Influence of temperature on percentages of extraction and recovery of (*S*)-amlodipine and the enantiomeric excess (% *e.e*)

6.5.3. Van't Hoff plots of distribution ratios (D_S, D_R)

The influences of temperature on the distribution behavior of (*R,S*)-amlodipine was investigated in the range between 278.15 K and 313.15 K. Table 6.3 shows that a higher temperature leads to an increase in distribution ratios.

Figure 6.6 show the variations of ln D_S and ln D_R versus $1/T$, respectively. The results can be described as matching very well with the Van't Hoff model. The higher temperature leads to an increase in distribution ratio because the non-selective physical partitioning is increasing with temperature [13, 15, 25]. However, the selectivity is reversed with increasing temperatures and it can be conclude that the selectivity of the enantiomeric complexation depend on the temperature.

Table 6.3 Influence of temperature on the enantioseparation parameters (D_S, D_R, α) of (*R*,*S*)-amlodipine.

Temperature (K)	D_S	D_R	α
278.15	1.74	1.01	1.72
283.15	2.08	1.28	1.63
288.15	2.42	1.59	1.52
293.15	3.01	2.24	1.34
298.15	3.61	2.91	1.24
303.15	4.21	3.55	1.19
308.15	5.32	4.90	1.09
313.15	6.09	6.05	1.01

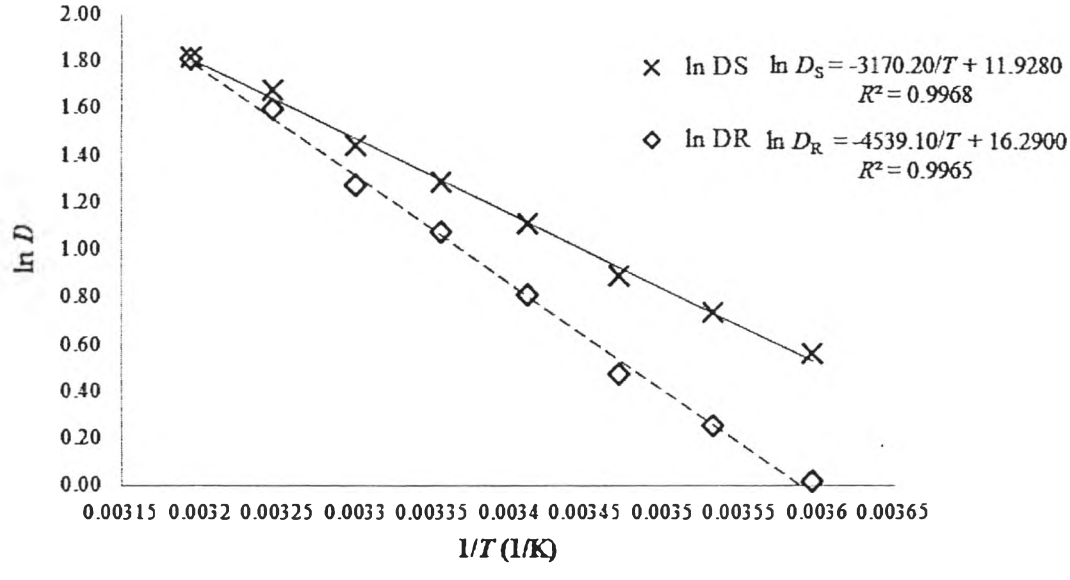

Figure 6.6 Van't Hoff's plots of distribution ratios (D_S) of (*S*)-amlodipine and (D_R) of (*R*)-amlodipine

6.5.4. Van't Hoff plots of enantioselectivities (α)

The influence of temperature on the enantioselectivities (α) of (*R*,*S*)-amlodipine was investigated in the range between 278.15 K and 313.15 K. Table 6.3 shows that a higher temperature leads to a decrease in enantioselectivities (α).

The variations of ln α versus $1/T$ are shown in Figure 6.7. The results can be described as matching very well with the Van't Hoff model, indicating that the

complexes do not change in conformation [66, 67] and that enantioselective interactions also do not change in the temperature range studied [66].

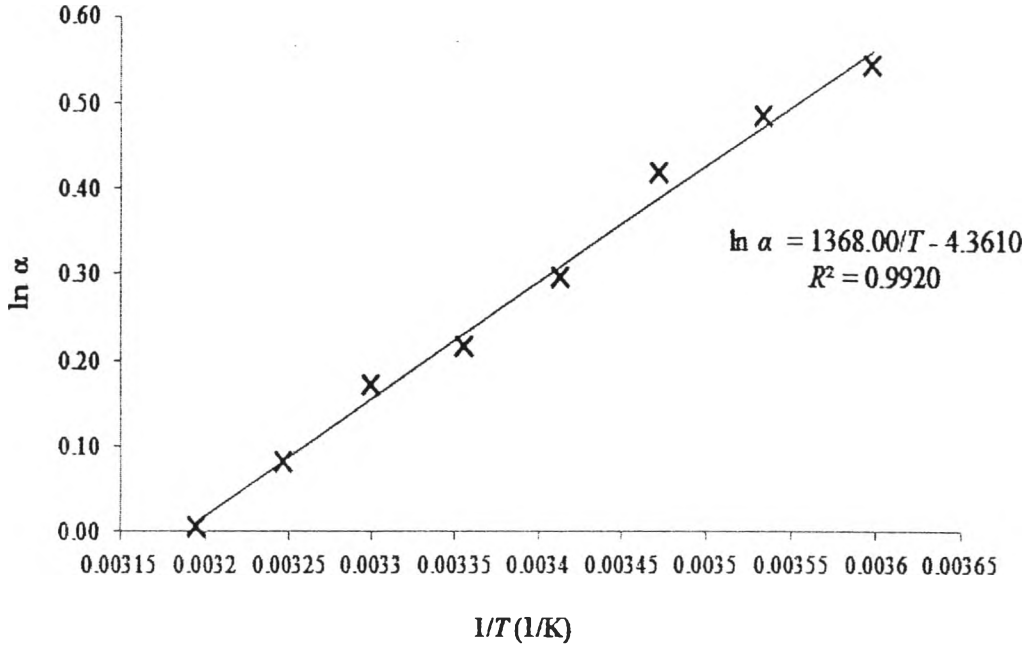

Figure 6.7 Van't Hoff plot of enantioselectivities (α)

6.5.5 Extraction equilibrium constant, the stripping equilibrium constant and the distribution ratio

The extraction equilibrium constant ($K_{ex(S)}$) for (*S*)-amlodipine extraction was calculated by the slope of the graph in Figure 6.8, and was found to be 1.3160 $(L/mmol)^2$ at 303.15 K. The extraction equilibrium constant ($K_{ex(S)}$) for (*S*)-amlodipine extraction values at temperature ranging from 278.15 K to 313.15 K were calculated by Eq. (6.3), as shown in Table 6.4.

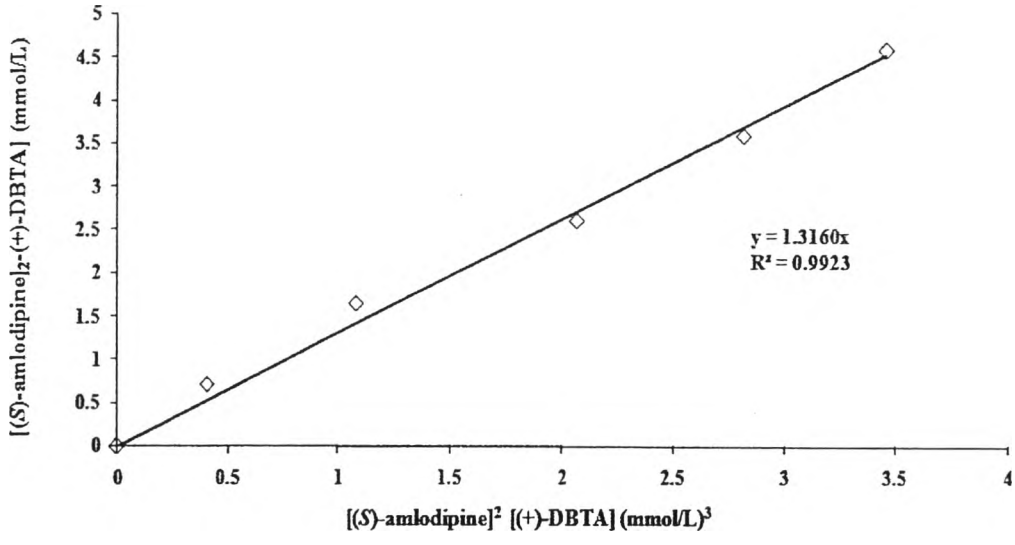

Figure 6.8 (*S*)-amlodipine extraction with (+)-DBTA as a function of equilibrium [(*S*)-amlodipine]^2[(+)-DBTA]

Table 6.4 Influence of temperature on extraction equilibrium ($K_{ex(S)}$), aqueous mass transfer coefficient (k_f) and membrane mass transfer coefficient (k_m)

Temperature (K)	$K_{ex(S)}$	Slope	Interception	k_m	k_f
278.15	1.0240	24.56	35.20	0.0356	0.0284
283.15	1.0840	25.04	35.45	0.0330	0.0282
288.15	1.1440	25.52	35.70	0.0307	0.0280
293.15	1.2040	26.01	35.95	0.0286	0.0278
298.15	1.2640	26.49	36.20	0.0267	0.0276
303.15	1.3160	26.97	36.45	0.0252	0.0274
308.15	1.3680	27.45	36.75	0.0238	0.0272
313.15	1.4200	27.93	36.95	0.0226	0.0271

6.5.6 The influence of temperature on extraction equilibrium

According to Eq. (6.15) and Eq. (6.17), the Van't Hoff equation was plotted in terms of ln ($K_{ex(S)}$) or ln ($K_{ex(R)}$) versus $1/T$ and considered as a function of temperature increasing from 278.15 K to 313.15 K. The HFSLM system used the condition of (+)-DBTA concentration at 4 mmol/L. The feed flow rate and stripping flow rate equaled 100 mL/min. The result for (*S*)-amlodipine extraction is shown in Figure 6.9. The values of $\Delta H^0_{ex(S)}$ and $\Delta S^0_{ex(S)}$ for (*S*)-amlodipine extraction were 6.7697 kJ/mol and 24.6026 J/(mol·K), respectively.

The positive value of $\Delta H^0_{ex(S)}$ indicates that the extraction process is an endothermic system. The positive value of $\Delta S^0_{ex(S)}$ and the negative value of $\Delta G^0_{ex(S)}$ indicated that the reaction process is a forward reaction. Their values from analytical calculations are shown in Table 6.5.

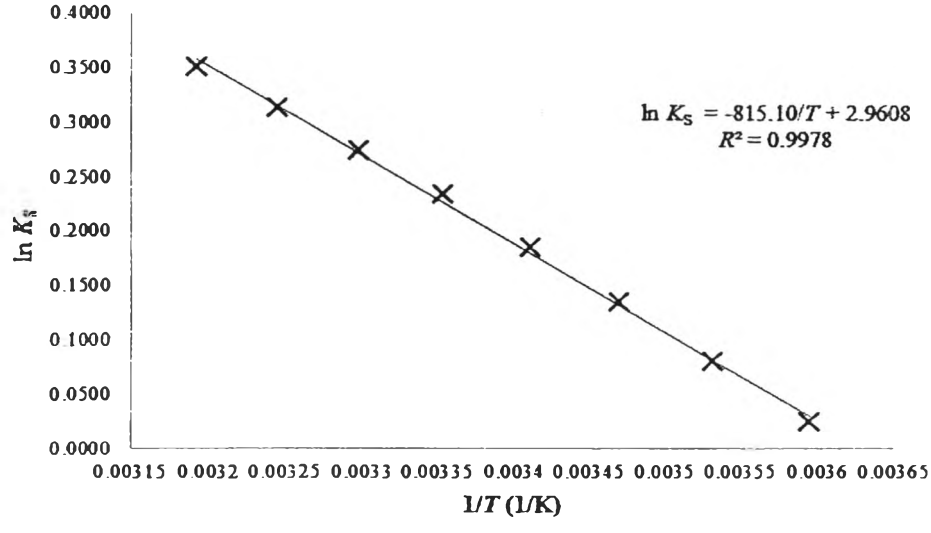

(a)

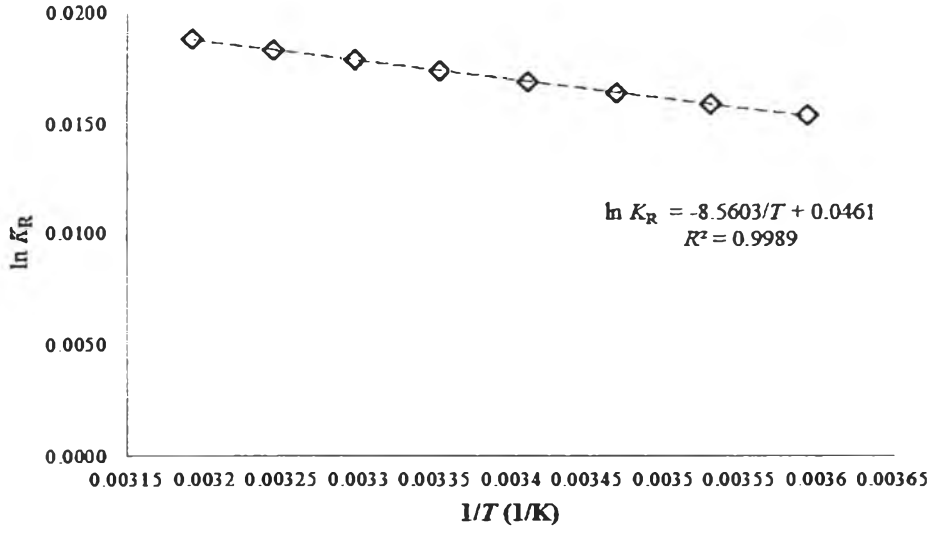

(b)

Figure 6.9 Van't Hoff's plots of the equilibrium constant: (a) (*S*)-amlodipine; (b) (*R*)-amlodipine

Table 6.5 Thermodynamic data for (*S*)-amlodipine extraction across a hollow fiber supported liquid membrane

Temperature (K)	$K_{ex(S)}$	$\Delta G_{ex(S)}$ (J/mol)	$\Delta H_{ex(S)}$ (kJ/mol)	$\Delta S_{ex(S)}$ (J/(mol-K))
278.15	1.0240	-69.8228		
283.15	1.0840	-192.8358		
288.15	1.1440	-315.8488		
293.15	1.2040	-438.8618	6.7697	24.6026
298.15	1.2640	-561.8748		
303.15	1.3160	-684.8878		
308.15	1.3680	-807.9008		
313.15	1.4200	-930.9138		

6.5.7 Permeability and mass-transfer coefficients

The permeability coefficient depends on the mass-transfer resistance, which is the reciprocal of the mass-transfer coefficients as calculated by Eq. (6.20). The value of the liquid-membrane permeability coefficient (P_m) from Eq. (6.22) is substituted into Eq. (6.20), assuming that the stripping reaction of (*S*)-amlodipine was instantaneous and there was no contribution from the stripping phase. Eq. (6.23) was used to calculate the aqueous mass-transfer coefficient (k_f) and the membrane mass-transfer coefficient (k_m). By plotting $1/P$ as a function of $1/[(S)\text{-amlodipine}]_f$ $[(+)\text{-DBTA}]_m$ for different carrier concentrations of (+)-DBTA, a straight line with the slope of $r_i/(r_{lm} \cdot K_{ex} \cdot k_m)$ and the ordinate of $1/k_f$ for the calculation is obtained (Figure 6.10 a-b). Thus, the values of k_f and k_m were found. The results are shown in table 6.4.

When the temperatures were lower than 293.15 K, the membrane mass-transfer coefficient (k_m) was less than the aqueous-feed mass-transfer coefficient (k_f). We can thus conclude that the mass-transfer across the membrane phase is the mass transfer-controlling step. However, when the temperature was higher than 293.15 K, the aqueous-feed mass-transfer coefficient (k_f) was less than the membrane mass-transfer coefficient (k_m). .

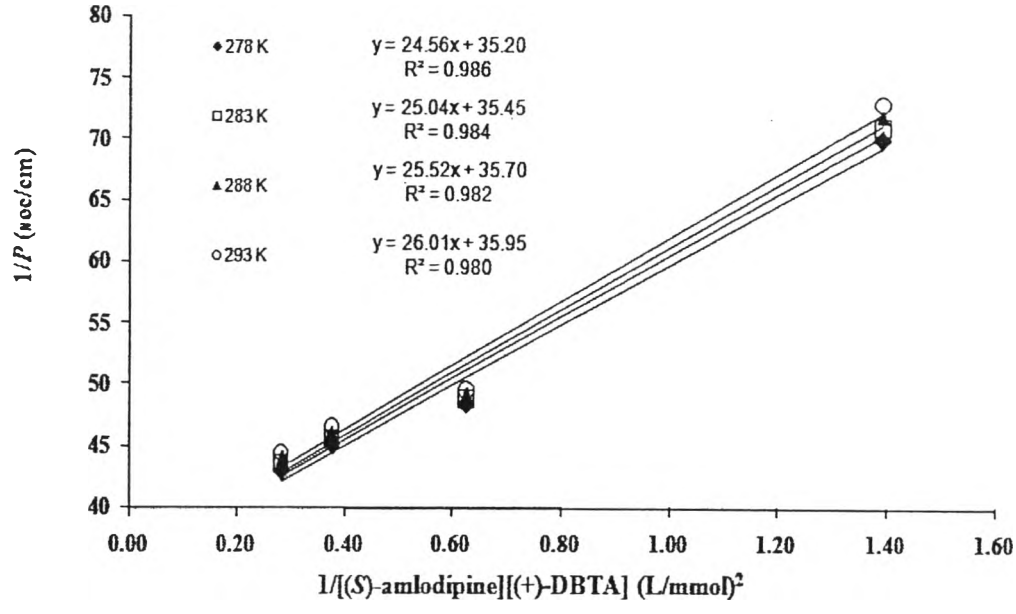

(a)

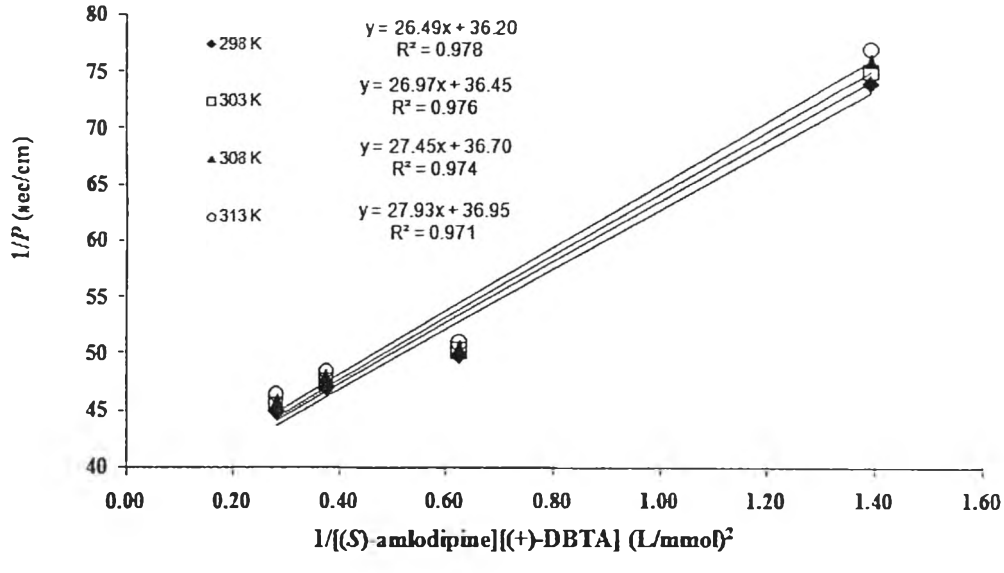

(b)

Figure 6.10 (a) Plot of $1/P$ as a function of $1/[(S)\text{-amlodipine}]_f\,[(+)\text{-DBTA}]_m$ at temperature 278-293 K; (b) Plot of $1/P$ as a function of $1/[(S)\text{-amlodipine}]_f\,[(+)\text{-DBTA}]_m$ at temperature 298-313 K.

6.5.8 Arrhenius plot of (*S*)-amlodipine transport

The effect of temperature on the transport of (*S*)-amlodipine across the HFSLM were tested at 278.15, 283.15, 288.15, 293.15, 298.15, 303.15, 308.15 and 313.15 K. It is clear that the flux of (*S*)-amlodipine increases with an increase in temperature. An Arrhenius-type plot is followed perfectly in Figure 6.11. The activation energy (E_a) of (*S*)-amlodipine was calculated as 71.10 kJ/mol from the slope of the curve, as presented Figure 6.10. These results show that the chemical reaction-controlled process is the rate-limiting step. The E_a values are somewhat higher with a chemically controlled process. For this reason, activation energy is used as an indicator of the control step of the chemical reaction during the HFSLM process. For chemical reaction controlled processes, E_a values are more than 40 kJ/mol. However, according to the literature on chemically controlled processes, E_a values are higher than 40 kJ/mol [59, 68]. Thus, the transport of (*S*)-amlodipine is considered to be the chemical reaction kinetics transport control regime. However, little information is available in the literature about the activation energy of the permeation of a component through a liquid membrane [69].

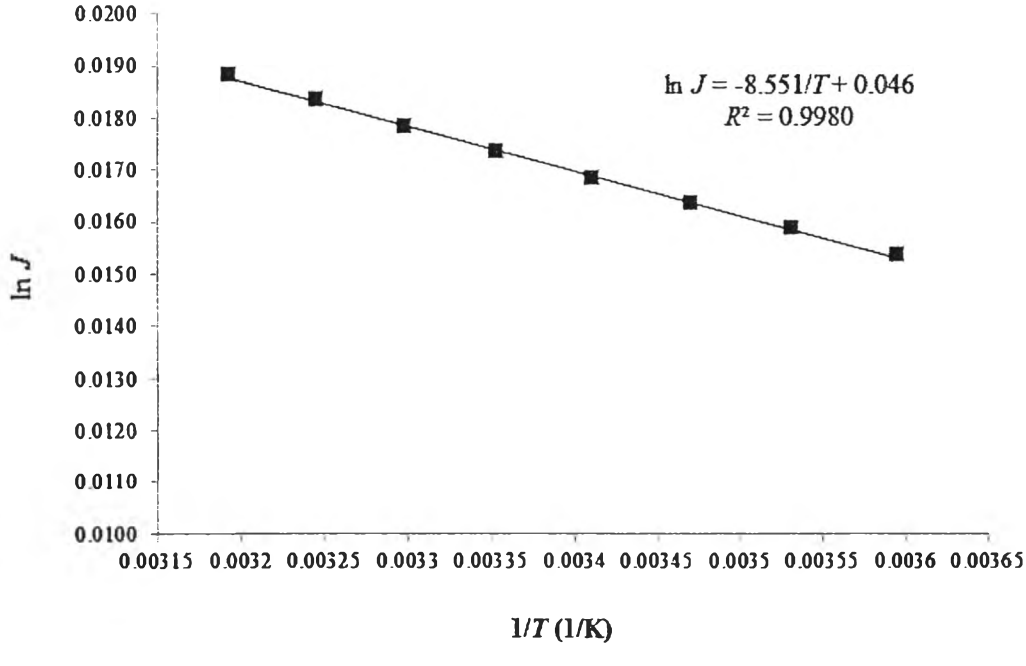

Figure 6.11 Arrhenius plot of (*S*)-amlodipine transport

6.6 CONCLUSIONS

This study highlighted that the influence of temperature on mass transfer in a single hollow-fiber membrane module depends on the factors that limit the transport. These can be categorized into feed-controlled, membrane-controlled and stripping-controlled types. As a practical aspect of these factors, temperature is a powerful variable for controlling and adjusting the enantioselectivity of (*S*)-amlodipine. The activation energy of the (*S*)-amlodipine extraction reaction was calculated as 71.10 kJ/mol. These results show that the chemical reaction controlled process is the rate-limiting step in the transport of (*S*)-amlodipine.

This work demonstrates that temperature has an important impact on the mass transfer of (*S*)-amlodipine across a hollow fiber supported liquid membrane. The temperature strongly affects D_S, D_R, and α, as well as $K_{ex(S)}$ and $K_{ex(R)}$ values. The results demonstrate energy-economic benefits offered by HFLSM extraction and the technique's potential to improve other industrially relevant chiral separations.

6.7 REFERENCES

[1] Abernethy, D.R. The pharmacokinetic profile of amlodipine. Am. Heart. J. 118 (1989): 1100-1103.

[2] Mason, R.P., Walter, M.F., Trumbore, M.W., Olmstead Jr., E.G., Mason, P.E. Membrane antioxidant effects of the charged dihydropyridine calcium antagonist amlodipine. J. Mol. Cell. Cardiol. 31 (1999): 275–281.

[3] Park, J.Y., Kim, K.A., Park, P.W., Lee, O.J., Ryu. J.H., Lee, G.H., Ha, M.C., Kim, J.S., Kang, S.W., Lee, K.R. Pharmacokinetic and pharmacodynamic characteristics of a new *S*-amlodipine formulation in healthy Korean male subjects: a randomized, open-label, two-period, comparative, cross over study. Clin. Ther. 28 (2006): 1837-1847.

[4] Lee, H.W., Shin, S.J., Yu, H., Kang, S.K., Yoo, C.L. A novel chiral resolving reagent, bis ((S)-mandelic acid)-3-nitrophthalate, for amlodipine racemate resolution: Scalable synthesis and resolution process. Org. Process Res.Dev. 13 (2009): 1382-1386.

[5] Yinghua, S., Liang, F., Meng, Z., Wei, L., Ping, M., Li, L., Zhonggui, H. A drug-in-adhesive transdermal patch for *S*-amlodipine free base: In vitro and in vivo characterization. Int. J. Pharm. 382 (2009): 165-171.

[6] Breuer, M., Ditrich, K., Habicher, T., Hauer, B., Kesseler, M., Sturmer, R., Zelinski, T. Industrial methods for the production of optically active intermediates. Angew. Chem. Int. 43 (2004): 788–824.

[7] Gotrane, D.M., Deshmukh, R.D., Ranade, P.V., Sonawane, S.P., Bhawal, B.M., Gharpure, M.M., Gurjar, M.K., A novel method for resolution of amlodipine. Org. Process Res.Dev. 13 (2010): 640–643.

[8] Streel, B., Laine, C., Zimmer, C., Sibenaler, R., Ceccato, A. Enantiomeric determination of amlodipine in human plasma by liquid chromatography coupled to tandem mass spectrometry. J. Biochem. Biophys. Methods 54 (2002): 357-368.

[9] Zandkarimi, M., Shafaati, A., Foroutan, S.M., Lucy, C.A. Rapid enantioseparation of amlodipine by highly sulfated cyclodextrins using short-end injection capillary electrophoresis. DARU 17(4) (2009): 269- 276.

[10] Goldmann, S., Stoltefuss, J., Born, L. Determination of the absolute configuration of the active amlodipine enantiomer as (-)-*S*: A correction. J. Med. Chem. 35 (1992): 3341-3344.

[11] Luksa, J., Josic, D.J., Podobnik, B., Furlan, B., Kremser, M. Semi-preparative chromatographic purification of the enantiomers *S*-(-)-amlodipine and *R*-(+)-amlodipine. J. Chromatogr. B. 693 (1997): 367-375.

[12] Schuur, B., Winkelman, J.G.M., Heeres, H.J. Equilibrium studies on enantio selective liquid-liquid amino acid extraction using a cinchona alkaloid Extractant. Ind. Eng. Chem. Res. 47 (2008) 10027-10033.

[13] Tang, K.W., Yi, J.M., Liu, Y.B., Jiang, X.Y., Pan, Y. Enantioselective separation of R,S-phenylsuccinic acid by biphasic recognition chiral extraction. Chem. Eng. Sci. 64 (2009) 4081-4088.

[14] Steensma, M., Kuipers, N.J.M., de Haan, A.B., Kwant, G. Identification of enantioselective extractants for chiral separation of amines and amino alcohols. Chirality 18 (2006) 314-328.

[15] Tang, K.W., Chen, Y.Y., Huang, K.L., Liu, J.J. Enantioselective Resolution of chiral aromatic acids by biphasic recognition chiral extraction. Tetrahedron: Asymmetry. 18 (2007) 2399-2408.

[16] Tang, K.W., Zhang, P.L., Pan C.Y., Li, H.J. Equilibrium studies on enantioselective extraction of oxybutynin enantiomers by hydrophilic-β-cyclodextrin derivatives, AIChE J. 57 (2011) 3027-3036.

[17] Maximinia, A., Chmiel, H., Holdikb, H. N.W. Maierc, Development of a supported liquid membrane process for separating enantiomers of N-protected amino acid derivatives, J. Membr. Sci. 276 (2006) 221–231.

[18] Dzygiel, P., Wieczorek, P.P. Supported liquid membranes and their modifications: definition, classifications, theory, stability, application and perspectives, in: V.S. Kislik (Ed.), Liquid Membranes, Elsevier, pp. 72–140.Amsterdam, 2010.

[19] Tang, K.W., Cai, J., Zhang, P.L. Equilibrium and Kinetics of Reactive Extraction of Ibuprofen Enantiomers from Organic Solution by HP-*β*-CD. Ind. Eng. Chem. Res. 51 (2012), 964–971.

[20] Tang, K.W., Zhang, P.L. Experimental and modeling studies on the enantioselective extraction of hydrophobic pranoprofen enantiomers with hydrophilic-*β*-cyclodextrin as selector. J. Chem. Eng. Data. 56 (2011) 3902-3909.

[21] Tang, K.W., Zhang, P.L., Li, H.J. Experimental and model study on the multiple chemical equilibrium for reactive extraction of ibuprofen enantiomers with HP-β-CD as hydrophilic selector. Process Biochem. 46 (2011) 1817-1824.

[22] Newcomb, M., Toner, J.L., Helgeson, R.C., Cram, D.J. Host-Guest Com plexation. 20. Chiral recognition in transport as a molecular basis for a catalytic resolving machine, J. Am. Chem. Soc. 101 (1979) 4941–4947.

[23] Schuur, B., Winkelman, J.G.M.,.de Vries, J.G., Heeres, H.J. Experimental and modeling studies on the enantioseparation of 3,5-dinitrobenzoyl-(R),(S)-leucine by continuous liquid-liquid extraction in a cascade of centrifugal contactor separators. Chem. Eng. Sci. 65 (2010) 4682–4690.

[24] Schuur, B., Verkuijl, B.J., Minnaard, A.J., de Vries, J.G., Heeres, H.J., Feringa, B.L. Chiral separation by enantioselective liquid-liquid extraction, Org. Biomol. Chem. 9 (2011) 36–51.

[25] Tang, K.W., Chen, Y.Y., Liu, J.J. Resolution of Zopiclone enantiomers by biphasic recognition chiral extraction. Sep. Purif. Technol. 62 (2008) 681-686.

[26] Pancharoen, U., Somboonpanya, S., Chaturabul, S., Lothongkum, A.W. Selective removal of mercury as $HgCl_4^{2-}$ from natural gas well produced water by TOA via HFSLM. J. Alloy Compd. 489 (2010): 72-79.

[27] Alguacil, F.J., Alonso, M., López, F.A., López-Delgado, A., Padilla, I., Tayibi, H. Pseudo-emulsion based hollow fiber with strip dispersion pertraction of iron (III) using $(PJMTH^{+})_2(SO_4^{2-})$ ionic liquid as carrier. Chem. Eng. J. 157 (2010): 366–372.

[28] Ren, Z.Q., Zhang, W.D., Li, H.S., Lin, W. Mass transfer characteristics of citric acid extraction by hollow fiber renewal liquid membrane. Chem. Eng. J. 146 (2009): 220–226.

[29] Vilt, M.E., Winston Ho, W.S. Supported liquid membranes with strip dispersion for the recovery of Cephalexin. J. Membr. Sci. (2009): 80–87.

[30] Rios, G.M., Belleville, M.P., Paolucci, D., Sanchez, J. Progress in enzymatic membrane reactors - a review. J. Membr. Sci. 242 (2004): 189–196.

[31] Wang, Z., Cai, C., Lin, Y., Bian, Y., Guo, H., Chen, X. Enantioselective separation of ketoconazole enantiomers by membrane extraction. Sep. Purif. Technol. 79 (2011): 63–71.

[32] Viegas, R.M.C., Afonso, C.A.M., Crespo, J.G., Coelhoso, I.M. Modelling of the enantioselective extraction of propranolol in a biphasic system, Sep. Purif. Technol. 53 (2007): 224–234.

[33] Kocherginsky, N.M., Yang, Q., Seelam, L. Recent advances in supported liquid membrane technology. Sep. Purif. Technol. 53 (2007): 171-177.

[34] Lothongkum, A.W., Suren, S., Chaturabul, S., Thamphiphit, N., Pancharoen, U. Simultaneous removal of arsenic and mercury from natural-gas-co-produced water from the Gulf of Thailand using synergistic extractant via HFSLM. J. Membr. Sci. 369 (2011): 350-358.

[35] Rogers, J.D., Long Jr., R.L. Modeling hollow fiber membrane contactors using film theory, Voronoi tessellations, and facilitation factors for systems with interface reactions. J. Membr. Sci. 134 (1997): 1–17.

[36] Zhang, W., Cui, C., Ren, Z., Dai, Y., Meng, H. Simultaneous removal and recovery of copper(II) from acidic wastewater by hollow fiber renewal liquid membrane with LIX984N as carrier. Chem. Eng. J. 157 (2010): 230-237.

[37] Giorno, L., Drioli, E. Enantiospecific membrane processes. Membrane Technol. 106 (1999): 6-11.

[38] Lothongkum, A.W., Panchareon, U., Prapasawat, T. Treatment of heavy metals from industrial wastewaters using hollow fiber supported liquid membrane, in Demadis, K. (Ed.), Water Treatment Processes, pp. 299-332. New York: Nova Science Publishers, 2012.

[39] Kandwal, P., Dixit, S., Mukhopadhyay, S., Mohapatra, P. K. Mass transport modeling of Cs(I) through hollow fiber supported liquid membrane containing calix-[4]-bis(2,3-naptho)-crown-6 as the mobile carrier. Chem. Eng. J. 174 (2011): 110-116.

[40] Chimuka, L., Nindi, M.M., ElNour, M.E.M., Frank, H., Velasco, C. Temperature-dependence of supported-liquid-membrane extraction, J. High Resolut. Chromatogr. 22 (1999): 417–420.

[41] Saf, A.O., Alpaydin, S., Sirit, A. Transport kinetics of chromium(VI) ions through a bulk liquid membrane containing p-tert-butyl calix[4]arene 3-morpholino propyl diamide derivative. J. Membr. Sci. 283 (2006): 448–455.

[42] Yimaz, A., Kaya, A., Alpoguz, H.K., Ersoz, M., Yilmaz, M. Kinetic analysis of chromium(VI) ions transport through a bulk liquid membrane containing p-tert-butylcalix[4]arene dioxaoctylamide derivative. Sep. Purif. Technol. 59 (2008): 1-8.

[43] Grosz, A., Heintz, A. Diffusion coefficients of aromatics in nonporous PEBA membranes. J. Membr. Sci. 168 (2000): 233–242.

[44] Chimuka, L. Michel, M. Cukrowska, E. Buszewski, B. Influence of temperature on mass transfer in an incomplete trapping supported liquid membrane extraction of triazole fungicides. J. Sep. Sci. 32 (2009): 1043–1050.

[45] Kazusaki, M., Kawabata H., Matsukura, H. Influence of temperature on enantioseparation employing an amylase-derivative stationary phase. J. Liquid Chromatogr. Relat. Technol. 23 (2000): 2937–2946.

[46] Tang, K.W., Song, L.T., Liu, Y.B., Jiang, X.Y., Pan, C.Y. Separation of flurbiprofen enantiomers by biphasic recognition chiral extraction. Chem. Eng. J. 158 (2010): 411-417.

[47] Schuur, B., Hallett, A.J., Winkelman, J.G.M., de Vries, J.G., Heeres, H.J. Scalable enantioseparation of amino acid derivatives using continuous liquid–liquid extraction in a cascade of centrifugal contactor separators. Org. Process Res.Dev. 13 (2009): 911–914.

[48] Prasad, R., Sirkar, K.K. Dispersion-free extraction with microporous hollow fibre modules. AIChE J. 34 (1988): 177-188.

[49] Sunsandee, N., Leepipatpiboon, N., Ramakul, P., Pancharoen, U. The selective separation of (S)-amlodipine via a hollow fiber supported liquid membrane: modeling and experimental verification. Chem. Eng. J. 180 (2012): 299-308.

[50] Greiner, W., Neise, L., Stöcker, H. Thermodynamics and Statistical Mechanics. Berlin and Heidelberg: Springer-Verlag, 1995. pp. 101-111.

[51] Angulo-Brown, F., Arias-Hernández, L.A., Van't Hoff's Equation for endoreversible chemical reactions. J. Phys. Chem. 100 (1996): 9193–9195.

[52] Westland, A.D., Otu, E.O. The thermodynamics of extraction of some lanthanide and other ions by 2-ethylhexylhydrogen-p-phenylphosphonate. Solvent Extr. Ion Exch. 9 (1991): 607–621.

[53] Otu, E.O., Westland, A.D. The thermodynamics of extraction of some lanthanides and other ions by dinonylnaphthalenesulfonic acid. Solvent Extr. Ion Exch. 8 (1990): 827–842.

[54] Otu, E.O. The effect of temperature on the synergistic extraction of thorium(IV) and uranium(VI) by 2-ethylhexylphenyl phosphonic acid and micelles of dinonylnaphthalenesulfonic acid. Solvent Extr. Ion Exch. 16 (1998): 1161–1176.

[55] Otu, E.O. The thermodynamics of synergistic extraction of bismuth by 2-ethylhexyl phenylphosphonic acid and micelles of dinonyl naphthalene sulfonic acid. Thermochim. Acta 329 (1999): 117–121.

[56] Otu, E.O., Westland, A.D. Solvent extraction with organophosphonic mono-acidic esters. Solvent Extr. Ion Exch. 8 (1990): 759–781.

[57] Danesi, P.R. A simplified model for the coupled transport of metal ions through hollow-fiber supported liquid membranes. J. Membr. Sci. 20 (1984): 231-248.

[58] O'Hara, P.A., Bohrer, M.P. Supported liquid membranes for copper transport, J. Membr. Sci. 44 (1989): 273–281.

[59] Kislik, V.S. Carrier-Facilitated Coupled Transport Through Liquid Membranes: General Theoretical Considerations and Influencing Parameters, in Kislik V.S. (Ed.), Liquid Membranes, pp. 16–71. Amsterdam: Elsevier, 2010.

[60] Peng, P., Fane, A.G., Li, X.D. Desalination by membrane distillation adopting a hydrophilic membrane. Desalination 173 (2005): 45–54.

[61] Scheuplein, R.J. Analysis of permeability data for the case of parallel diffusion pathways. Biophysical J. 6 (1966): 1–17.

[62] İnce, E., Kõirbaşlar, Ş.İ. Liquid-liquid equilibria of the water-acetic acid-butyl acetate system. Braz. J. Chem. Eng. 19 (2002): 243–254.

[63] Lin, S.H., Juang, R.S. Mass-transfer in hollow fiber module for extraction and back-extraction of copper (II) with LIX64N carriers. J. Membr. Sci. 188 (2001) 251-262.

[64] Wannachod, P., Chaturabul, S., Pancharoen, U., Lothongkum, A.W., Patthaveekongka, W. The effective recovery of praseodymium from mixed rare earths via a hollow fiber supported liquid membrane and its mass transfer related. J. Alloy. Compd. 509 (2011): 354-361.

[65] Chung, Y.S., Ha, M.C. Resolution of the enantiomers of amlodipine. US Patent Application 2003/6646131 B2 (November 11, 2003).

[66] Kazusaki, M., Ohgami, Y., Enantioseparation in the Vicinity of Compensation Temperature on Amylose Tris (3,5-dimethylbenzoate) Chiral Stationary Phase. Chromatogr. 28 (2007): 125–130.

[67] Tang, K.W, Song, L., Liu, Y., Miao, J. Enantioselective partitioning of 2-phenylpropionic acid enantiomers in a biphasic recognition chiral extraction system. Chem. Eng. J. 180 (2012): 293-298.

[68] Aydiner, C., Kobya, M., Demirbas, E. Cyanide ions transport from aqueous solutions by using quaternary ammonium salts through bulk liquid membranes. Desalination 180 (2005): 139–150.

[69] Mohapatra, R., Kanungo, S.B., Sarma, P.V.R.B. Kinetics of the transport of Co (II) from aqueous sulfate solution through a supported liquid membrane containing di(2-ethylhexyl) phosphoric acid in kerosene. Sep. Sci. Technol. 27 (1992): 765–781.